ELSEVIER

Journal of Clinical Imaging 29 (2005) 235–245

CLINICAL IMAGING

Classification of breast ultrasound images using fractal feature

Dar-Ren Chen[a,*], Ruey-Feng Chang[b], Chii-Jen Chen[b], Ming-Feng Ho[b], Shou-Jen Kuo[a], Shou-Tung Chen[a], Shin-Jer Hung[c], Woo Kyung Moon[d]

[a]*Department of General Surgery, Changhua Christian Hospital, 135 Nanhsiao Street, Changhua 500, Taiwan*
[b]*Department of Computer Science and Information Engineering, National Chung Cheng University, Chiayi, Taiwan*
[c]*Department of General Surgery, China Medical University and Hospital, Taiwan*
[d]*Department of Diagnostic Radiology, Seoul National University Hospital, South Korea*

Received 30 September 2004; received in revised form 10 October 2004; accepted 2 November 2004

Abstract

Fractal analyses have been applied successfully for the image compression, texture analysis, and texture image segmentation. The fractal dimension could be used to quantify the texture information. In this study, the differences of gray value of neighboring pixels are used to estimate the fractal dimension of an ultrasound image of breast lesion by using the fractal Brownian motion. Furthermore, a computer-aided diagnosis (CAD) system based on the fractal analysis is proposed to classify the breast lesions into two classes: benign and malignant. To improve the classification performances, the ultrasound images are preprocessed by using morphology operations and histogram equalization. Finally, the *k*-means classification method is used to classify benign tumors from malignant ones. The US breast image databases include only histologically confirmed cases: 110 malignant and 140 benign tumors, which were recorded. All the digital images were obtained prior to biopsy using by an ATL HDI 3000 system. The receiver operator characteristic (ROC) area index A_Z is 0.9218, which represents the diagnostic performance.

Keywords: Fractal; Texture; Ultrasound; Box counting; Brownian motion; Fractal dimension; *k*-means classification

1. Introduction

Cancer remains a major public health problem in developed countries. Breast cancer is the most common cancer in women, accounting for nearly one out of every three cancers in the United States. In 2003, 211,300 women are expected to be diagnosed with this disease, and only lung cancer causes more deaths among women [1]. The early detection and diagnosis of breast cancer are the key to decrease death rate and to provide prompt treatment. Now, breast cancer is detected and diagnosed by a combination of physical examination, imaging, and biopsy [2,3]. Mammography and ultrasound are the main imaging techniques for breast cancer. Some patients with palpable breast cancers may have mammogram and sonogram examinations with both normal, benign, or nonspecific in appearance [4]. Up to date, to confirm whether a patient has breast cancer, it has to rely on biopsy. However, biopsy is one kind of invasive surgical operation and imposes both psychological and physical impacts on patients. To avoid unnecessary biopsy, many researches have investigated computer-aided diagnosis (CAD) systems [5–9] that offer more objective evidences and stable high diagnostic rates.

An ultrasonographic image consists of different values of gray-level intensity, and different tissues have markedly different texture. Benign lesions are classically described as regular masses with homogenous internal echoes, but malignant lesions are described as masses with fuzzy border and heterogeneous internal echoes [9]. In this paper, fractal characteristics are proposed to differentiate the benign and malignant lesions. There are several features that can distinguish the benign and malignant breast lesions. For

* Corresponding author. Tel.: +886 4 7238595; fax: +1 886 4 7267167.
E-mail address: dlchen88@ms13.hinet.net (D.-R. Chen).

0899-7071/05/$ – see front matter © 2005 Elsevier Inc. All rights reserved.
doi:10.1016/j.clinimag.2004.11.024

example, the often used diagnosis features in CAD systems are texture [6,8,9] and shape. This paper will focus on the study of texture feature. Texture refers to properties that represent the surface or structure of an object; it is widely used but has no precise definition due to its wide variability. Fractal geometry [10,11] can be used on occasion to discriminate between different textures. Fractal refers to entities, especially sets of pixels, which display a degree of self-similarity at different scales. Fractal analyses have been applied for several medical image applications [12–20]. Most of these fractal analysis researches are focused on digital mammograms [12–15,17–20]. Lefebvre et al. [18] presented a computerized method for the automated segmentation of individual microcalcifications in a region of interest (ROI) in digital mammograms. Zheng and Chan [17] presented an algorithm that combines several artificial intelligent techniques, including fractal dimension analysis, with the discrete wavelet transform for the detection of masses in mammograms. Pohlman et al. [15] proposed six different morphological descriptors, including fractal dimension, to distinguish benign and malignant breast lesions in digitized mammograms. The above fractal analysis methods are applied for the mammograms. However, Garra et al. [16] used fractal analysis and statistical texture analysis methods for the ultrasound images, to improve the ability of ultrasound to distinguish benign from malignant breast lesions. They concluded that the most useful features are the co-occurrence matrices of the ultrasound images, not the fractal analysis.

2. Materials and methods

Here, we briefly introduce three basic techniques to be used in the paper, morphology, histogram equalization, and *k*-means classification. Noise filtering and shape simplification are the main objectives of the morphology used in the image preprocessing. Because the breast tumor images are collected in different periods by different doctors for different patients, histogram equalization is adopted to make the US images at similar gray levels and good contrast for improving the classification performance. The *k*-means is a simple method for classifying the fractal features used in this paper into benign and malignant lesions.

2.1. Morphology

Digital morphology [21,22] behind the mathematics is simply set theory, which is a well-studied area. A small pattern or shape, which is known as structuring element, probes the image. Basic morphological operations are erosion and dilation. Erosion is an operation on the image that pixels matching a structuring element are deleted. For the dilation operation, the area about a pixel is set to a given structuring element and the original object to grow larger. The definitions of these operations are dependent on the types, including binary, gray level, or color, of the image being processed (see Appendix A).

2.2. Histogram equalization

The histogram of an image provides the frequency distribution of gray levels in that image. For example, the histogram of an 8-bit image can be represented by a table with 256 entries, or bin indexed form 0 to 255. In Bin 0, the number of times of a gray level of 0 occurring is recorded; in Bin 1, the number of times of a gray level of 1 occurring; and so on, up to Bin 255. Histogram equalization [21,23] is usually used for contrast enhancement, and it redistributes gray levels in an attempt to flatten the frequency distribution, as shown in Fig. 1 (see Appendix B).

2.3. k-means classification

The purpose of the *k*-means, also described by the names *c*-means or iterative relocation, is to partition the data into *k* clusters, so that within each group, the sum of squared error is minimized. That is, the *k*-means is a least-squares partitioning method allowing users to divide a collection of objects into *k* groups. Given *k*, e.g., $k=2$, we are able to classify the features that are gotten from fractal textures of breast tumor images to distinguish the benign from malignant breast tumors (see Appendix C).

2.4. Fractal texture description

Traditionally, the Euclidean objects [11], such as lines, planes, and circles, etc., have used as the basis of the intuitive understanding of the geometry of nature. However, most nature objects do not resemble Euclidean objects. With the help of fractal geometry, it is possible to model nature objects to a better description in many conditions. The concept of fractal was first introduced by Mandelbrot [24]. The main distinct difference between Euclidean and fractal geometry is that of self-similarity, which is described by nonuniform scaling. In theory, shapes of fractal objects keep invariant under successive magnifying or shrinking the objects. We have known that the texture is a problem of scale; that is, the texture description is scale dependent. Hence, the fractal geometry can be applied to overcome the scale problem of texture. Because the concept of fractal dimension is an indicator of the surface roughness and people usually describe texture as fine, coarse, gained, and

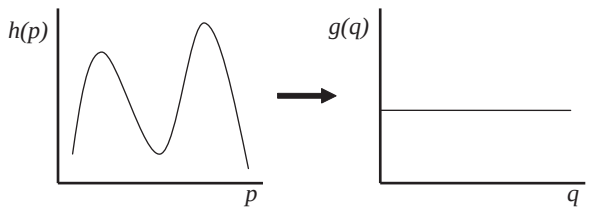

Fig. 1. Histogram equalization.

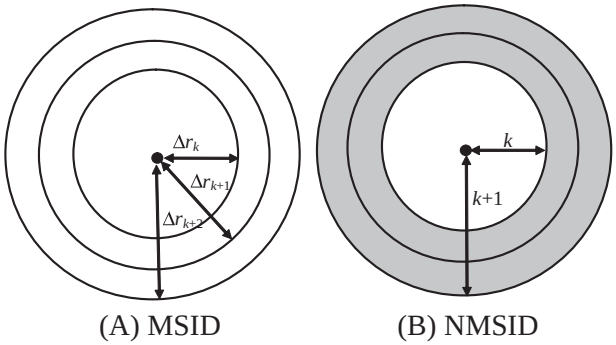

Fig. 2. (A) Multiscale intensity difference vector. $di(k)$ is computed by only the pixel pairs with distance Δr_k. The value of Δr_k may be fractional. (B) Normalized multiscale intensity difference vector. The value of k is an integer. $di(k)$ is computed by all the pixel pairs in the highlighted region.

smooth, etc., hence, it implies that fractal-based texture analysis is a correlation between texture coarseness. Fractal models typically relate a metric property, such as the length of a line or surface area, to the elementary length or area used as a basis for determining the metric property. For example, the coast length could be measured by applying a 1-km-long ruler end to end to the coastline. If a 0.5-km ruler or other short ruler is used for the same coast, then the measured length will be longer. The relation between the ruler length and the measured coast length can be considered a measure of the coastline's geometric properties, e.g., its roughness. This property can be found also in other naturally occurring objects. The functional relationship between ruler size ε and the measured length L is

$$L = \lambda \varepsilon^{1-D} \tag{1}$$

where λ is a scaling constant and D is the fractal dimension. In practice, D has been shown to correlate with the function's intuitive roughness.

A variety of procedures, including box counting, fractal Brownian motion [25–27], and fractal interpolation function system [11], have been proposed for estimating the fractal dimension of images. We mainly introduce the *fractional Brownian motion model with* gray-scale variation [25–27], which has shown promise in the medical image texture. The Brownian motion curve concepts can be extended to the fractional Brownian motion curve $I(x)$, and $|I(x2)-I(x1)|$ have a mean value proportional to $|(x2-x1)|^H$. Thus, in the fractal Brownian motion, there is only one parameter of interest, H, or the Hurst coefficient, which can be described as texture features, when we applied it to classify breast tumor images. Considering the topological dimension T_d, for images, $T_d=3$, the fractal dimension D can be estimated from the Hurst coefficient H as

$$H = T_d - D \tag{2}$$

For the medical images, the fractal dimension can be estimated from the above relationship. If we define

$$\Delta r = \sqrt{(x2-x1)^2+(y2-y1)^2}, \Delta I_{\Delta r} = |I(x2,y2)-I(x1,y1)|$$

then a simple way to estimate fractal dimension is to use the following equation:

$$E\left(\Delta I_{\Delta r}\right) = k(\Delta r)^H = k(\Delta r)^{3-D} \tag{3}$$

where $E()$ is an expectation operator, $\Delta I_{\Delta r}$ is the intensity variation, Δr is the spatial distance, and $k=E(\Delta I)_{\Delta r=1}$ is the scaling constant, and by applying the log function to both sides of the equation, we can deduce

$$\log(E(\Delta I_{\Delta r})) = H\log(\Delta r)+\log k. \tag{4}$$

Because $\log k$ is a constant, the parameter H can be deduced from the least-squares linear regression to estimate the slope of the gray value differences $\log(E(\Delta I_{\Delta r}))$ versus $\log(\Delta r)$ by choosing $\Delta r_{\max}$ and $\Delta r_{\min}$.

Given an $M\times M$ image I, the implementation of estimation fractal dimension [25] can be defined as

$$di(k) = \frac{\sum_{x1=0}^{M-1}\sum_{y1=0}^{M-1}\sum_{x2=0}^{M-1}\sum_{y2=0}^{M-1}|I(x2,y2)-I(x1,y1)|}{\mathrm{pn}(k)} \tag{5}$$

where $\mathrm{pn}(k)$ is the total number of pixel pairs with distance

$$\Delta r_k = \sqrt{(x2-x1)^2+(y2-y1)^2} \text{ and}$$
$$f(k) = \log(di(k))-\log(di(1)) \quad \text{for } k=1,2,\ldots,n. \tag{6}$$

The vector $[di(1), di(2), \ldots, di(n)]$ is called the multiscale intensity difference (MSID) vector, and the vector $[f(1), f(2),\ldots, f(n)]$ is called the factional Brownian motion feature (FBM) vector. For example, in Fig. 2(A), $di(k)$ is computed by only the pixel pairs with distance Δr_k, and the value of Δr_k may be fractional. Because the total number of all possible scales is too large, Chen et al. [25] also proposed a normalized multiscale intensify difference (NMSID) vector. In this normalized method, only the integer scales are used. That is, all the pixel pairs $(x1,y1)$ and $(x2,y2)$ with $k\le\sqrt{(x2-x1)^2+(y2-y1)^2}<k+1$ are used to compute the value of $di(k)$ in Eq. (5). As shown in Fig. 2(B), $di(k)$ is computed by all the pixel pairs in the highlighted region.

From the above discussion, a perfect fractal intensity surface, $f(k)=H\log(\Delta r_k)$, and the H can be obtained. Fractal dimension D is then derived from the values of the Hurst

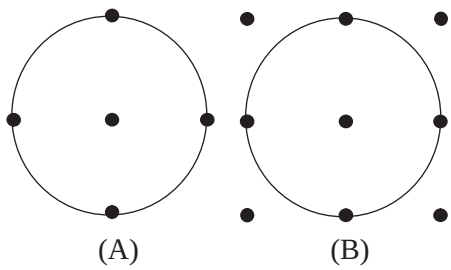

Fig. 3. (A) Only the pixel pairs with horizontal or vertical distance k are used to compute $di(k)$. (B) The pixel pairs with horizontal, vertical, diagonal, and asymmetric–diagonal directions are used to compute $di(k)$.

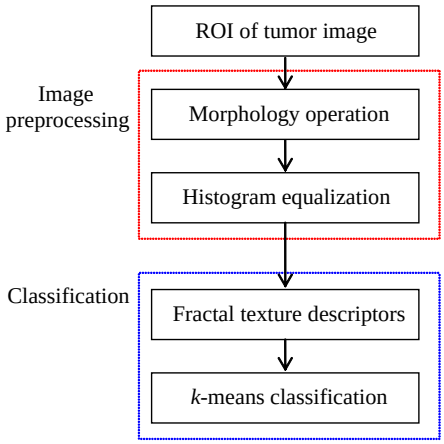

Fig. 4. Flowchart of processing.

coefficients. A small value of the fractal dimension, i.e., a large value of H, represents a fine texture, while a large fractal dimension corresponds to a coarse texture.

However, the drawback of Eq. (5) is that it tends to be time consuming; this algorithm needs M^4 operations for estimating the fractal dimension of an image of size $M\times M$. Thus, Wu et al. [26] proposed the modified method using only the gray level differences between the pixel pairs with horizontal or vertical distance k, as shown in Fig. 3(A). That is, the $di(k)$ is redefined as

$$di(k)=\frac{\sum_{x=0}^{M-1}\sum_{y=0}^{M-k-1}|I(x,y)-I(x,y+k)|+\sum_{x=0}^{M-k-1}\sum_{y=0}^{M-1}|I(x,y)-I(x+k,y)|}{2M(M-k)} \tag{7}$$

Then, Chen et al. [27] proposed another modified method using the gray-level differences between the pixel pairs with horizontal, vertical, diagonal, and asymmetric–diagonal directions, as shown in Fig. 3(B). The $di(k)$ is redefined as

$$di(k)=\left[\begin{array}{l}\sum_{x=0}^{M-1}\sum_{y=0}^{M-k-1}\left|I(x,y)-I(x,y+k)\right|/M(M-k)\\ +\sum_{y=0}^{M-1}\sum_{x=0}^{N-k-1}\left|I(x,y)-I(x+k,y)\right|/M(M-k)\\ +\sum_{x=0}^{M-k-1}\sum_{y=0}^{M-k-1}\left||I(x,y)-I(x+k,y+k)\right|/(M-k)^2\\ +\sum_{x=0}^{M-k-1}\sum_{y=0}^{M-k-1}\left|I(x,M-y)-I(x+k,M-(y+k))\right|/(M-k)^2\end{array}\right]/4 \tag{8}$$

3. The proposed fractal analysis method

The fractal analysis method is proposed for diagnosis of tumors in sonograms, and the flowchart of the proposed method is illustrated as Fig. 4. In the first subsection, how to acquire the image data is introduced. Then, the procedure for the image

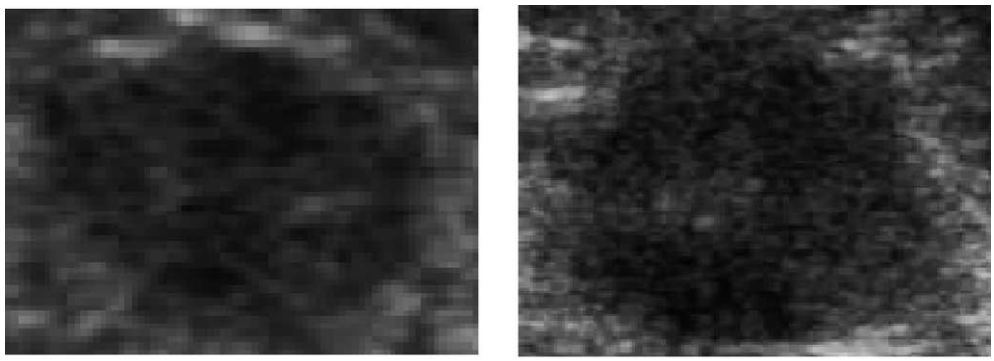

(A) (B)

Fig. 5. Original tumor images. (A) Benign. (B) Malignant.

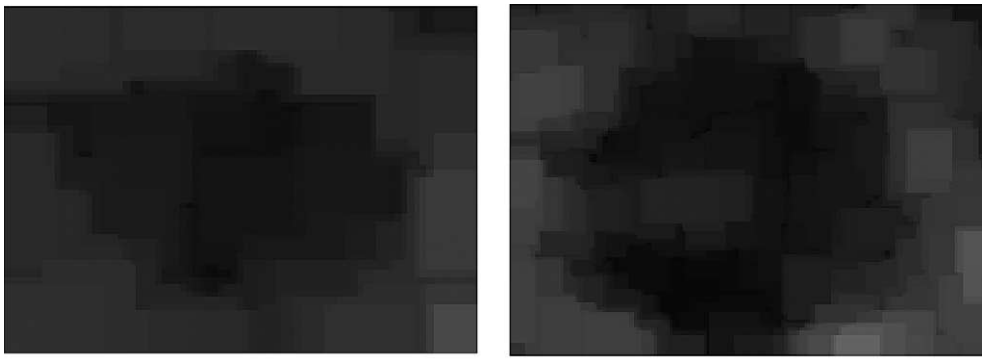

Fig. 6. Morphological operation. (A) Benign. (B) Malignant.

preprocessing is described to remove the noise in the US images and to make the US images at similar gray levels and good contrast for improving the classification performance of the proposed fractal analysis method. Finally, we describe the extraction of texture features using the proposed fractal method.

3.1. Data acquisition

The US breast image databases include only histologically confirmed cases: 110 malignant tumors and 140 benign tumors, which were recorded from August 1, 1999, to May 31, 2000. The ages of the patients ranged from 18 to 64 years. All the digital images were obtained prior to biopsy using by an ATL HDI 3000 system with a L10-5 small part transducer, which is a linear-array transducer with a frequency of 5–10 MHz and a scan width of 38 mm. During the US scanning, no acoustic standoff pad was used. All the images were supplied by one of the authors (Dr. Moon). The ROI that contains the tumor was selected by one of the authors (Dr. Chen). Throughout this study, only the ROI subimages are used to investigate the texture characteristics of benign and malignant lesions. Note that only one lesion is extracted from a patient.

3.2. Image preprocessing

Image preprocessing methods were used to remove the redundancy in images for improving the image data with undesired noisy or to enhance some image features that is important for further processing. Images are inherent of randomness. The US images typically have randomness connected with both the nature of the fundamental structure and the random noise superimposed on the image. In the previous section, we have mentioned that the fractal analysis is sensitive to the noise. To continue the study, we need to eliminate the noise through the procedure of image preprocessing. Several methods can be used to eliminate the noise in image processing, including median filter, averaging, and mean filter, etc. In this paper, the morphological operations are used as an image filter to eliminate the noise; and those operations are the erosion and dilation operations. The structuring element is a nonflat ellipsoid shape whose radius in the X–Y plane is R and whose height is H. In this paper, $R=3$ and $H=3$. Fig. 5 shows the original benign and malignant images. Fig. 6 shows the results of the morphological operations for the images in Fig. 5.

The ROIs containing the tumors are very dissimilar in image sizes and different in gray levels. Therefore, another image processing method is needed to make the

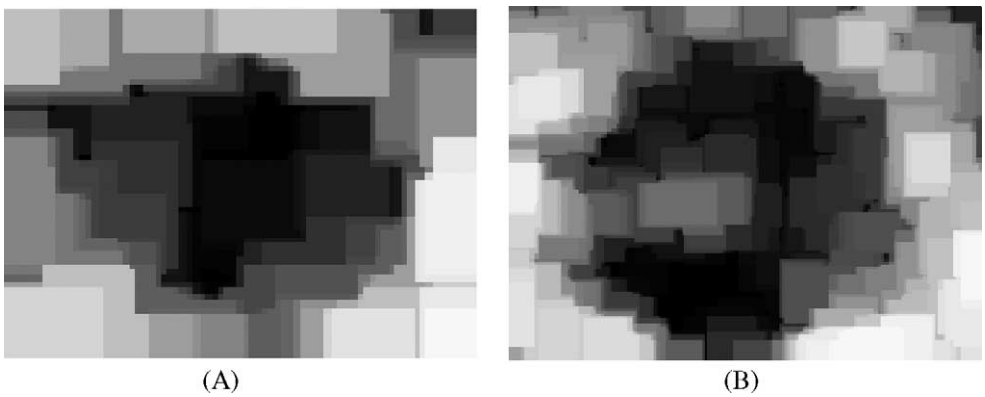

Fig. 7. Histogram equalization after morphological operation. (A) Benign. (B) Malignant.

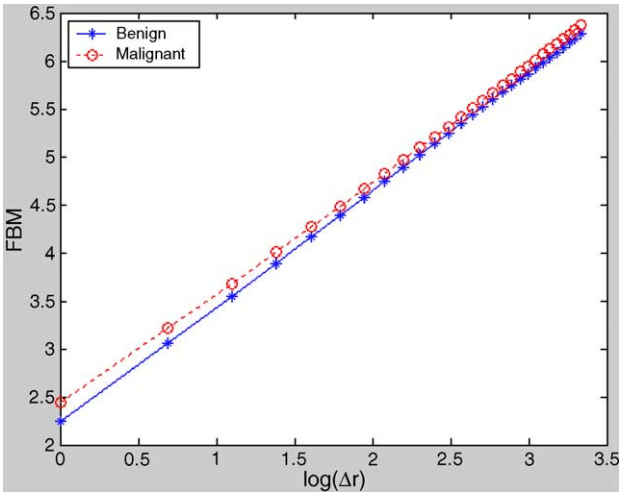

Fig. 8. Fractal analysis based on Wu's method for images in Fig. 6 without image preprocessing. The slope of the benign line is 0.2994, and the slope of the malignant is 0.3038.

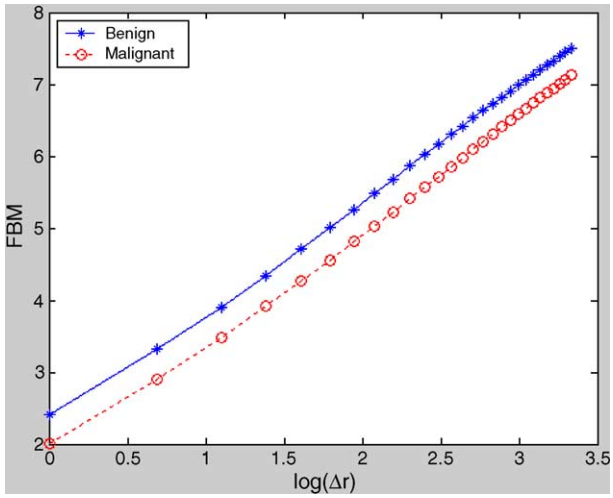

Fig. 10. Fractal analysis based on Wu's method for images in Fig. 7 with image preprocessing. The slope of the benign line is 0.3550, and the slope of the malignant is 0.3334.

images at comparable gray levels and good contrasts. In this paper, histogram equalization is used for the purpose. Fig. 7 is the result after the histogram equalization for the images in Fig. 6.

3.3. Fractal analysis

In the previous section, we have discussed the fractal texture descriptor for texture analysis. The authors [25] proposed the normalized MSID vectors to reduce the number of all possible scales to M for an image of size $M \times M$. However, the total number of all possible scales is still too large and a lot of time is needed to find the fractal dimension. There are two simpler MSID vectors [26,27] used to reduce the calculation time. In Wu's method [26], only the intensity differences of pixels pairs with horizontal or vertical distance k are needed to be found. The pixel pairs with distance k along horizontal, vertical, diagonal, and asymmetric–diagonal directions are needed to be found, their intensity differences proposed in the paper of Chen et al. [27]. Now, these two simpler MSID vectors are adopted in the following fractal analysis. The following figures demonstrate the fractal analysis for the benign and malignant US images in Figs. 6 and 7. In Figs. 8 and 9, the fractal analysis is applied for the US images without the image preprocessing. In Figs. 10 and 11, the fractal analysis is applied for those images after the morphology operations and the histogram equalization.

Note that the slopes of lines in Figs. 10 and 11 are the Hurst parameters H, and the fraction dimension can be deduced from $3-H$. According to the above figures, we can find that those two lines are more separated in Figs. 10

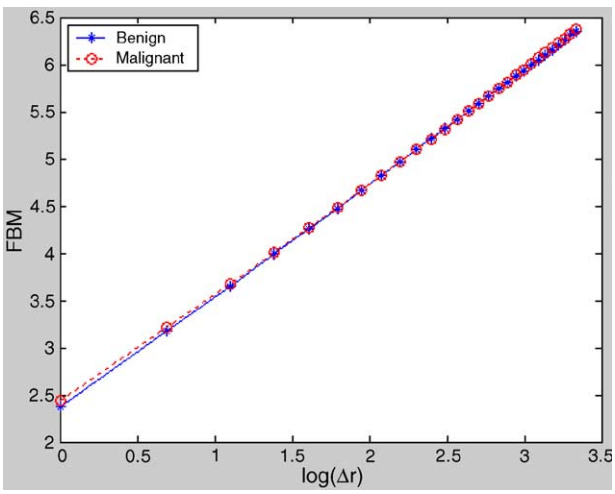

Fig. 9. Fractal analysis based on Chen's method for images in Fig. 6 without image preprocessing. The slope of the benign line is 0.3031, and the slope of the malignant is 0.3038.

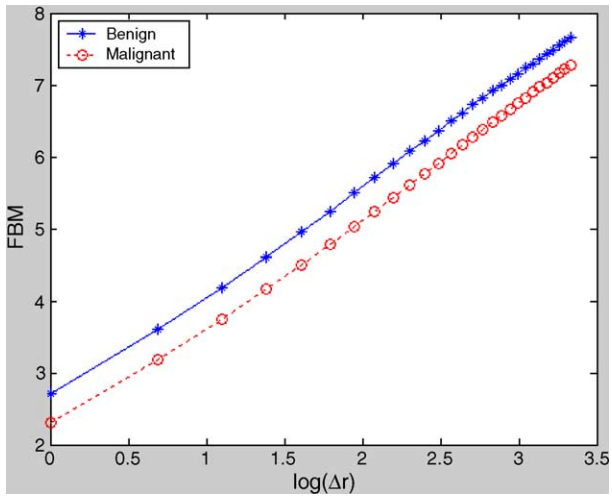

Fig. 11. Fractal analysis based on Chen's method for images in Fig. 7 with image preprocessing. The slope of the benign line is 0.3644, and the slope of the malignant is 0.3425.

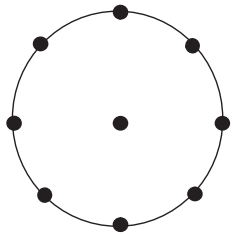

Fig. 12. The pixel pairs with horizontal, vertical, diagonal, and asymmetric–diagonal directions are used to compute $di(k)$. Note that the distance of all the pixel pairs are the same.

and 11 than those in Figs. 8 and 9. Moreover, the slope difference is larger in Figs. 10 and 11. Hence, the images with the preprocessing can obtain much better results of the fractal analysis. In the next section, more benign and malignant cases will be used to prove that the image preprocessing could improve the classification performance for fractal analysis. In this paper, we will propose another modified fractal analysis method. This method is based on the methods of Wu et al. [26] and Chen et al. [27]. Note that, in the method of Chen et al. [25], the distance of pixel pairs along the diagonal and asymmetric-diagonal is $\sqrt{2}k$, not k. Hence, according to the original definition of MSID, the equation for $id(k)$ is modified as

$$id(k)=\left[\begin{array}{l}\displaystyle\sum_{x=0}^{M-1}\sum_{y=0}^{M-k-1}\left|I(x,y)-I(x,y+k)\right|/M(M-k)\\ +\displaystyle\sum_{y=0}^{M-1}\sum_{x=0}^{N-k-1}\left|I(x,y)-I(x+k,y)\right|/M(M-k)\\ +\displaystyle\sum_{x=0}^{M-\frac{k}{\sqrt{2}}-1}\sum_{y=0}^{M-\frac{k}{\sqrt{2}}-1}\left|I(x,y)-I(x+\frac{k}{\sqrt{2}},y+\frac{k}{\sqrt{2}})\right|/(M-\frac{k}{\sqrt{2}})^2\\ +\displaystyle\sum_{x=0}^{M-\frac{k}{\sqrt{2}}-1}\sum_{y=0}^{M-\frac{k}{\sqrt{2}}-1}\left|I(x,M-y)-I(x+\frac{k}{\sqrt{2}},M-(y+\frac{k}{\sqrt{2}}))\right|/(M-\frac{k}{\sqrt{2}})^2\end{array}\right]/4 \quad (9)$$

The pixel pairs used in computing $id(k)$ are shown in Fig. 12. Note that the fractal dimension H can be obtained by estimating the slope of log(FBM) versus log(Δr) between $\Delta r_{\min}$ and $\Delta r_{\max}$ using the least-squares linear regression [25]. In the cases of Figs. 8–11, $\Delta r_{\min}$=1 and the $\Delta r_{\max}$=30. Fig. 13 is the results using our method for those images in Fig. 11. Note that H=0.3578 for the benign image and H=0.3351 for malignant image.

Hence, in this paper, the preprocessing techniques, morphological operations, and histogram equation are used at first to remove the image noise and to enhance the image contrast. The fractal analysis based on Eq. (9) is used to find the fractal dimension of the US images and the fractal dimension is used as the texture features for diagnosis. Finally, the k-means classification is used to classify the US images into benign and malignant cases.

4. Experiments and results

In this study, the hardware experiment environment is Intel Pentium III-800 with 512M RAM, and the programming environment is the MATLAB of MathWorks (Natick, MA, USA). The preprocessing techniques, morphology operations, and histogram equalization use the functions in the image toolbox.

From the flowchart Fig. 4, the proposed method could be divided into three main steps: morphology operation, histogram equalization, and fractal analysis. The first two steps are the preprocessing technique to obtain better fractal texture features. Actually, these two preprocessing steps are very important and necessary, and the results with and without will be compared. The fractal features are extracted by using our modified version in Eq. (9) to obtain the multiscale intensity difference vector [$di(1)$, $di(2)$,. . ., $di(n)$] with $\Delta r_{\min}$=1 and $\Delta r_{\max}$=8. After obtaining the multiscale intensity difference vector, the factional Brownian motion feature vector [$f(1)$, $f(2)$,. . ., $f(n)$] can be obtained by using Eq. (6), and then, the fractal dimension could be obtained by the slope of the factional Brownian motion feature vector versus log(Δr), estimated by the least-squares linear regression. Finally, the k-means classification method will be adopted to verify the classification result. For diagnosis purpose, the US images are divided into two classes, benign and malignant, i.e., k=2. The k-means is an unsupervised classification method and requires only the parameter of the classification group number, k. However, for the purpose of justification, we will apply the supervised manner to simulate the diagnosis process. Hence, in the classification experiments, the US images will be divided into the training and the test sets. The training set is used to build the k-means model, and the test set is used to verify the trained k-means model. Note that the cases in the test set are not used to train

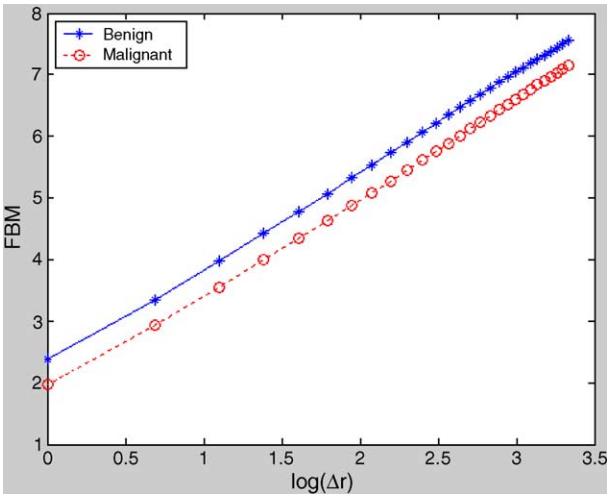

Fig. 13. Fractal analysis based on our method for images in Fig. 7 with image preprocessing. The slope of the benign line is 0.3578, and the slope of the malignant is 0.3351.

the *k*-means model. Due to that the number of the US images is not large, the cross-verification method is used, and the US images are divided into five groups. The first group is used as the test set and the remaining four groups are used as the training set. Next, the second is used as the test set and the remaining four groups are used as the training set. The above procedure is repeated until each group is used as the test set once. Note that the centers of two classes, benign and malignant, are obtained from the training set by using the *k*-means method. For diagnosis, if a test case is close to the center of the benign class, then this class is classified as benign. Otherwise, this case is classified as malignant. Tables 1 and 2 list the classification results for the fractal dimension and all fractal coefficients $f(i)$. Note that the classification performances of these fractal features are almost the same. In Table 2, five performance indexes, accuracy, sensitivity, specificity, positive predictive value (PPV), and negative predictive value (NPV), are adopted to evaluate the classification performance. The accuracy of the proposed fractal analysis is 88.80%.

Because the fractal dimension and the third fractal coefficient $f(3)$ have slightly better results, the following comparisons will focus on these two features. At first, the results with and without the preprocessing steps are compared. The distribution of these features with the preprocessing steps is shown in Figs. 14 and 15, and the distribution of these features without the preprocessing steps is shown in Figs. 16 and 17. In Figs. 14 and 15, the benign and malignant classes are clearly separated. However, these two classes cannot be separated in Figs. 16 and 17. Hence, we can prove that the preprocessing steps are very important and necessary.

Table 2
Summary of performance among fractal texture features

	Fractal dimension [%]	$f(1)$ [%]	$f(2)$ [%]	$f(3)$ [%]	$f(4)$–$f(7)$ [%]
Accuracy	88.80	88.40	88.80	88.80	88.80
Sensitivity	93.64	92.72	92.73	93.64	93.64
Specificity	84.29	85.00	85.71	85.00	84.29
PPV	82.40	82.92	83.61	83.06	82.40
NPV	94.40	93.70	93.75	94.40	94.40

Accuracy=(TP+TN)/(TP+TN+FP+FN); Sensitivity=TP/(TP+FN); Specificity=TN/(TN+FP); Positive Predictive Value (PPV)=TP/(TP+FP); Negative Predictive Value (NPV)=TN/(TN+FN).

At last, the receiver operator characteristic (ROC) curve is used to evaluate the fractal feature. The software package LABROC1 by Professor C.E. Metz, University of Chicago, is used to fit the ROC curve. The performance of the diagnosis feature can be evaluated by examining the ROC area index, A_Z. The ROC curve for the fractal dimension is shown in Fig. 18. The ROC area index A_Z is up to 0.9218.

5. Discussion

Many texture features can be used in computer-aided schemes. Fractal analysis is a useful one. The input image is the ROI subimage containing the lesion selected by a physician. After, the preprocessing technique is applied for the ROI image to remove the noise and enhance the contrast. Then, the fractal analysis is applied to obtain the fractal texture features to classify the test cases into benign and malignant. From the experimental results, the fractal analysis is useful to represent the texture information of US breast lesions. The accuracy rate of the proposed system is up to 88.80%.

In the future researches, this fractal analysis technique could be applied for other medical images or other image preprocessing techniques. More advanced nonlinear classification methods such as neural network or fuzzy logic can be used to improve the classification accuracy. Now, the ROI is selected by a physician. For the convenient of

Table 1
Classification of breast tumors by *k*-means with fractal texture descriptors

Fractal texture	The fractal dimension		The first fractal coefficient $f(1)$		The second fractal coefficient $f(2)$		The third fractal coefficient $f(3)$		The fourth fractal coefficient $f(4)$		The fifth fractal coefficient $f(5)$		The sixth fractal coefficient $f(6)$		The seventh fractal coefficient $f(7)$	
Benign	TN118	FN 7	TN 119	FN 8	TN 120	FN 8	TN 119	FN 7	TN 118	FN 7	TN 118	FN 7	TN 118	FN 7	TN 118	FN 7
Malignant	FP 22	TP 103	FP 21	TP 102	FP 20	TP 102	FP 21	TP 103	FP 22	TP 103	FP 22	TP 103	FP 22	TP 103	FP 22	TP 103
Total	140	110	140	110	140	110	140	110	140	110	140	110	140	110	140	110

TP: true positive; TN: true negative; FP: false positive; FN: false negative.

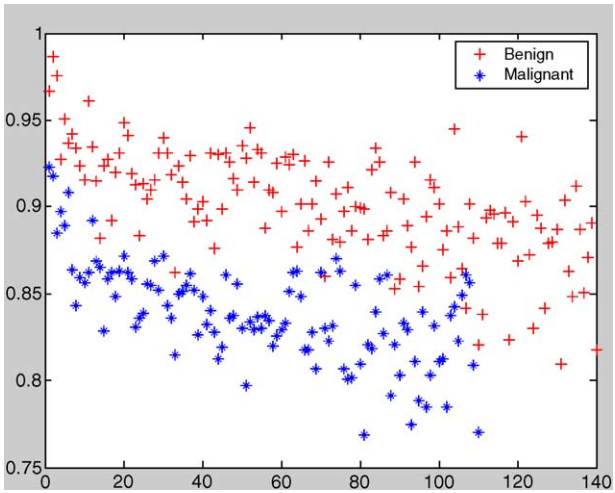

Fig. 14. The fractal dimension for the ROIs images with morphology operations and histogram equalization. The horizontal axis is the case number.

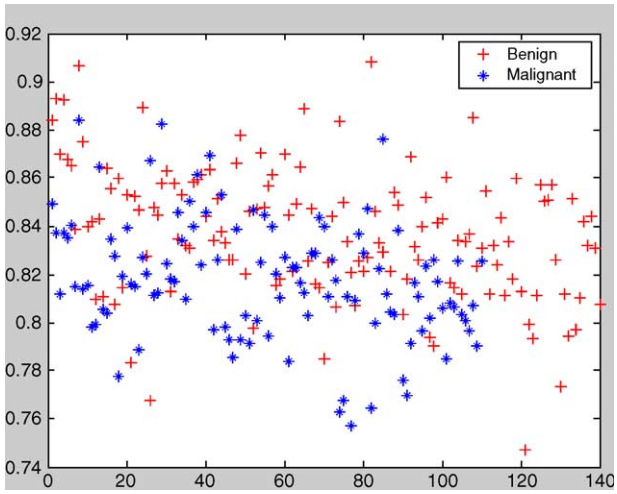

Fig. 16. The fractal dimension for the ROIs images without morphology operations and histogram equalization. The horizontal axis is the case number.

clinical usage, we try to develop an automatic detection and segmentation method from an ultrasonic image. Furthermore, the segmentation method could be added to the proposed system to find the tumor contour, and only the texture information inside the tumor is used to diagnose the tumor. In the future, we will extend the fractal analysis for 3D US images based on our experiences of 2D fractal analysis and 3D US to compare their performances.

Appendix A

First, we introduce the morphological operations for binary images and then mainly consider those operations for the gray-level images because the breast tumor image is also a gray-level image.

The structuring element is a small matrix of pixels. When a morphological operation is carried out, the origin of the structuring element is typically translated to each current processing pixel position in the image, in turn, and then the pixels within the translated structuring element are compared with the underlying image pixel values. Next, the two relations fit or hit, between the structuring element, and the processed image needs to be defined. It is said that a structuring element to fit an image if, for all the pixels in the structuring element being set to 1, their corresponding image pixels are also 1. On the contrary, if there is at least one structuring pixel being set to 1 and its corresponding

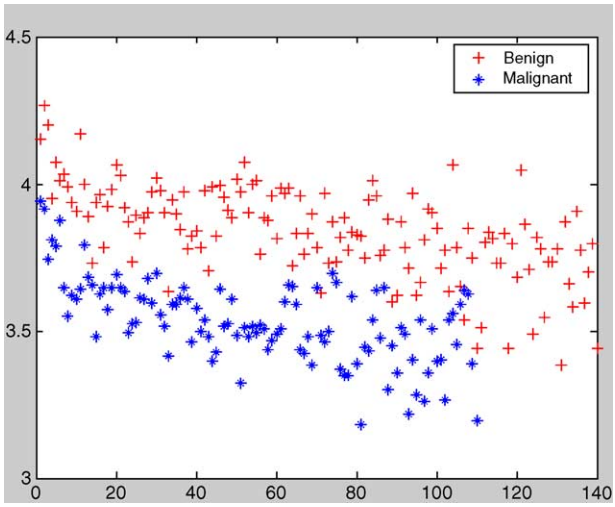

Fig. 15. The third fractal coefficient $f(3)$ for the ROIs images with morphology operations and histogram equalization. The horizontal axis is the case number.

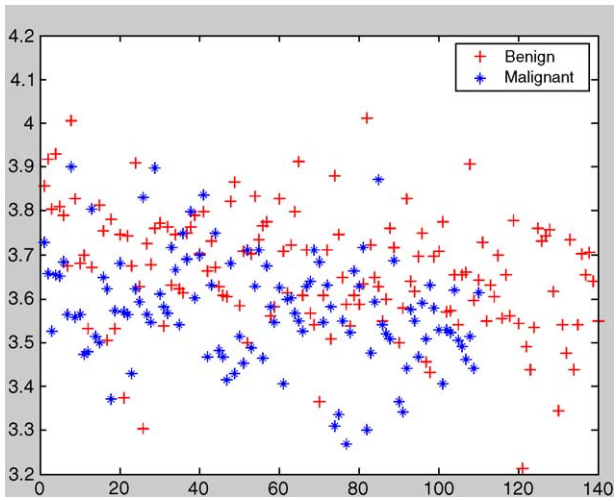

Fig. 17. The third fractal coefficient $f(3)$ for the ROIs images without morphology operations and histogram equalization. The horizontal axis is the case number.

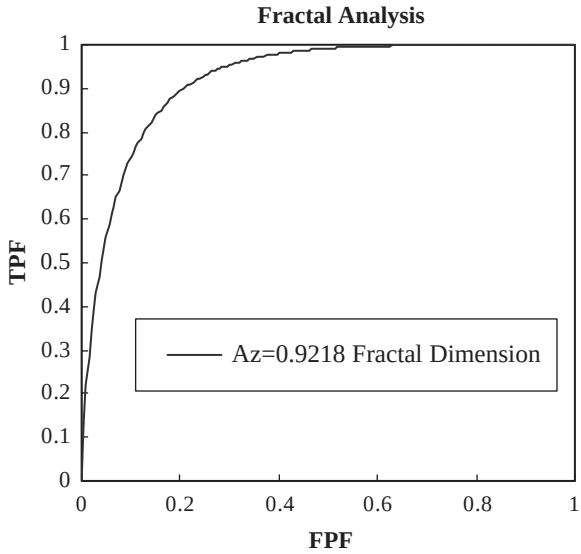

Fig. 18. The ROC analysis of the fractal dimension feature.

image pixel being also 1, then this structure element is said to hit the image. Then, the dilation of an image f by a structuring element s is denoted $g=f\oplus s$ by applying the following rule for the current processing pixel (x,y)

$$g(x,y)=\begin{cases}1 & \text{if } s \text{ hits } f,\\ 0 & \text{otherwise,}\end{cases}$$

The erosion of an image f by a structure element s is written $g=f\ominus s$ by applying the following rule to the current processing pixel (x,y)

$$g(x,y)=\begin{cases}1 & \text{if } s \text{ fits } f,\\ 0 & \text{otherwise,}\end{cases}$$

Fig. 19 illustrates the morphology on the given structuring element and images. In the figure, the structuring element defines the neighborhood of the pixel of interest that is circled.

Morphological image processing is not restricted to binary images. Actually, the binary morphological operations acting on binary images could be easily extended to the gray level images using the *min* and *max* operations.

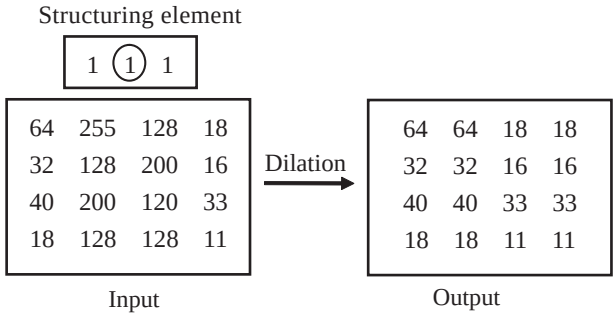

Fig. 20. Dilation of a gray-level image.

Denoting an image by f and a structuring element by s, the gray scale dilation at a pixel (x,y) is

$$(f\oplus s)(x,y)=\max[f(x+i,\ y+j)-s(i,j)]$$

where i and j are the indexes for the pixels of s, as shown in Fig. 20. The gray scale erosion is equivalent to

$$(f\ominus s)(x,y)=\min[f(x+i,\ y+j)-s(i,j)].$$

where i and j are the indexes for the pixels of structuring element.

Appendix B

Let the original image be $f(x,y)$ and the processed image after the histogram equalization be $g(x,y)$. The following algorithm shows how this work in practice.

Step 1. Calculate a scaling factor $\alpha=(2^n-1)/N$, where n is the number of bits for a pixel and N is the total number of pixels in $f(x,y)$. For an 8-bit image, $\alpha=255/N$.

Step 2. Compute the histogram $h[i]$, where i is all possible gray levels in $f(x,y)$. For an 8-bit gray level image, i is from 0 to 255.

Step 3. Let the accumulated histogram be $c[i]$ and $c[0]=\alpha\times h[0]$. For all gray levels i, do $c[i]=c[i-1]+\alpha\times h[i]$.

Step 4. For all pixels (x,y), do $g(x,y)=c[f(x,y)]$.

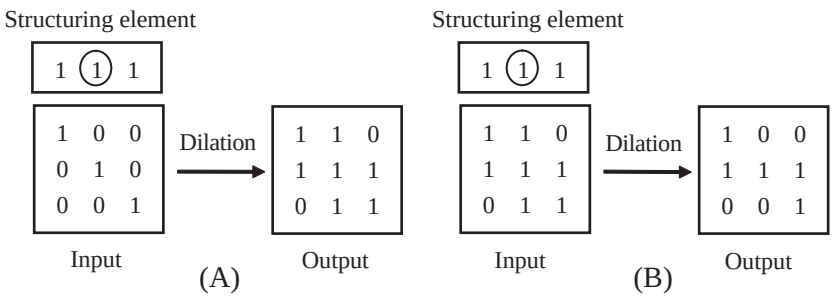

Fig. 19. Morphology of a binary image. (A) Dilation. (B) Erosion.

Appendix C

Let the input vectors be X_1, X_2,..., X_p. The k-means algorithm is defined as follows.

Step 1. For all cluster c, set total[c]=(0,0,...,0), count[c]=0, and center[c]=a random vector. For all input vector i, set belong[i]=0 and old-belong[i]=1.

Step 2. Let min_dis be the maximum value of integer. For each input vector X_i
For each cluster j=1 to k
d_{ij}=the distance of X_i to center[j]
If d_{ij}<min_dis then min_dis=d_{ij}
belong[i]=j
total[j]=total[j]+X_i
count[j]=count[j]+1

Step 3. If all old-belong[i]=belong[i], then stop.

Step 4. For all i, old-center[i]=belong[i]. For all clusters j, center[j]=total[j]/count[j], total[j]=(0,0,...,0), count[j]=0 and go to Step 2.

References

[1] Jemal A, Murray T, Samuels A, Ghafoor A, Ward E, Thun MJ. Cancer statistics, 2003. CA Cancer J Clin 2003;53(1):5–26.

[2] Esserman LJ. New approaches to the imaging, diagnosis, and biopsy of breast lesions. Cancer J 2002;8(Suppl 1):S1–S14.

[3] Shetty MK, Shah YP. Prospective evaluation of the value of negative sonographic and mammographic findings in patients with palpable abnormalities of the breast. J Ultrasound Med 2002;21(11): 1211–6.

[4] Beyer T, Moonka R. Normal mammography and ultrasonography in the setting of palpable breast cancer. Am J Surg 2003;185(5): 416–9.

[5] Kuo WJ, Chang RF, Chen DR, Lee CC. Data mining with decision trees for diagnosis of breast tumor in medical ultrasonic images. Breast Cancer Res Treat 2001;66(1):51–7.

[6] Chen DR, Chang RF, Kuo WJ, Chen MC, Huang YL. Diagnosis of breast tumors with sonographic texture analysis using wavelet transform and neural networks. Ultrasound Med Biol 2002;28(10): 1301–10.

[7] Kuo WJ, Chang RF, Lee CC, Moon WK, Chen DR. Retrieval technique for the diagnosis of solid breast tumors on sonogram. Ultrasound Med Biol 2002;28(7):903–9.

[8] Chang RF, Wu WJ, Moon WK, Chen DR. Improvement in breast tumor discrimination by support vector machines and speckle-emphasis texture analysis. Ultrasound Med Biol 2003;29(5):679–86.

[9] Chen DR, Chang RF, Huang YL. Computer-aided diagnosis applied to US of solid breast nodules by using neural networks. Radiology 1999;213(2):407–12.

[10] Pentland A. Fractal-based description of natural scenes. IEEE Trans Pattern Anal Mach Intell 1984;6(6):661–74.

[11] Fortin C, Kumaresan R, Ohley W, Hoefer S. Fractal dimension in the analysis of medical images. IEEE Eng Med Biol 1992;11(2):65–71.

[12] Heine JJ, Deans SR, Velthuizen RP, Clarke LP. On the statistical nature of mammograms. Med Phys 1999;26(11):2254–65.

[13] Caldwell CB, Stapleton SJ, Holdsworth DW, Jong RA, Weiser WJ, Cooke G, Yaffe MJ. Characterisation of mammographic parenchymal pattern by fractal dimension. Phys Med Biol 1990;35(2):235–47.

[14] Thiele DL, Kimme-Smith C, Johnson TD, McCombs M, Bassett LW. Using tissue texture surrounding calcification clusters to predict benign vs malignant outcomes. Med Phys 1996;23(4):549–55.

[15] Pohlman S, Powell KA, Obuchowski NA, Chilcote WA, Grundfest-Broniatowski S. Quantitative classification of breast tumors in digitized mammograms. Med Phys 1996;23(8):1337–45.

[16] Garra BS, Krasner BH, Horii SC, Ascher S, Mun SK, Zeman RK. Improving the distinction between benign and malignant breast lesions: the value of sonographic texture analysis. Ultrason Imag 1993;15(4):267–85.

[17] Zheng L, Chan AK. An artificial intelligent algorithm for tumor detection in screening mammogram. IEEE Trans Med Imag 2001;20(7):559–67.

[18] Lefebvre F, Benali H, Gilles R, Kahn E, Di Paola R. A fractal approach to the segmentation of microcalcifications in digital mammograms. Med Phys 1995;22(4):381–90.

[19] Li H, Liu KJ, Lo SC. Fractal modeling and segmentation for the enhancement of microcalcifications in digital mammograms. IEEE Trans Med Imag 1997;16(6):785–98.

[20] Velanovich V. Fractal analysis of mammographic lesions: a prospective, blinded trial. Breast Cancer Res Treat 1998;49(3):245–9.

[21] Gonzalez RC, Woods RE. Digital image processing. 2nd ed. Upper Saddle River (NJ): Prentice-Hall, 2002.

[22] Parker JR. Algorithms for image processing and computer vision. New York: Wiley, 1997.

[23] Sonka M, Hlavac V, Boyle R. Image processing: analysis and machine vision. 2nd ed. Pacific Grove (CA): PWS Publishing, 1999.

[24] Mandelbrot BB. Fractal geometry of nature. New York: W H Freeman & Co, 1983.

[25] Chen CC, Daponte JS, Fox MD. Fractal feature analysis and classification in medical imaging. IEEE Trans Med Imag 1989; 8(2):133–42.

[26] Wu CM, Chen YC, Hsieh KS. Texture features for classification of ultrasonic liver images. IEEE Trans Med Imag 1992;11(2):141–52.

[27] Chen EL, Chung PC, Chen CL, Tsai HM, Chang CI. An automatic diagnostic system for CT liver image classification. IEEE Trans Biomed Eng 1998;45(6):783–94.